Research Article

Aneela Anwar*, Ayesha Sadiqa, Azeem Intisar, Amin Ur Rashid, Tabassam Razaq, Samar A. Aldossari, Mohammed Sheikh Saleh Mushab, Dong Yong Park*, and Dongwhi Choi*

Synergistic effect of hydroxyapatite-magnetite nanocomposites in magnetic hyperthermia for bone cancer treatment

https://doi.org/10.1515/ntrev-2023-0225
received November 21, 2023; accepted February 24, 2024

Abstract: Hydroxyapatite/magnetite (HA-Fe_3O_4) nanocomposite materials that have the synergistic ability to produce heat when in direct bonding with a bone through HA are regarded competent hyperthermia therapies of bone carcinoma treatment. HA-Fe_3O_4 nanocomposites with various magnetite concentrations (10, 20, and 30 wt%) were quickly synthesized using a novel continuous microwave-assisted flow synthesis (CMFS) process in a 5 min residence duration at the conditions of pH 11. In this process, initially, phase pure hydroxyapatite and superparamagnetic magnetite nanoparticles followed by a series of HA-Fe_3O_4 nanocomposites were formed, without a subsequent aging step. The obtained nano-product was physically analyzed using Brunauer-Emmett-Teller (BET) surface area analysis, transmission electron microscopy, and X-ray powder diffraction analysis. X-ray photoelectron spectroscopy was used for the chemical structure analysis of the final nanocomposite product. Zeta potential measurements were carried out to determine colloidal stability associated with the surface charge of the nanocomposites. The magnetic properties were determined using a vibrating sample magnetometer. The results indicated the high magnetization property of the obtained nanoproduct, suitable for hyperthermia application. HA-Fe_3O_4 nanocomposites have shown remarkable antimicrobial properties against *E. coli* and *S. cerevisiae*. Thus, the CMFS system facilitated the rapid production of HA-Fe_3O_4 nanocomposite particles with fine particle size.

Keywords: continuous flow synthesis, hydroxyapatite, hyperthermia, magnetite, nanocomposite, synergistic effect

*** Corresponding author: Aneela Anwar,** Department of Chemistry, University of Engineering and Technology, GT Road, Lahore, Pakistan, e-mail: a.anwar@uet.edu.pk
*** Corresponding author: Dong Yong Park,** Advanced Mobility Components Group, Korea Institute of Industrial Technology, 320 Techno sunhwan-ro, Yuga-eup, Dalsung-gun, Republic of Korea, e-mail: vbeena013@gmail.com
*** Corresponding author: Dongwhi Choi,** Department of Mechanical Engineering (Integrated Engineering Program), Kyung Hee University, 1732 Deogyeong-daero, Yongin, Gyeonggi, 17104, Republic of Korea, e-mail: dongwhi.choi@khu.ac.kr
Ayesha Sadiqa: Department of Chemistry, The University of Lahore, 1-Km Defence Road, Near Bhuptian Chowk, Lahore, Punjab, Pakistan
Azeem Intisar: School of Chemistry, University of Punjab, Quaid-e-Azam Campus, Lahore, Punjab, Pakistan
Amin Ur Rashid: Department of Physical and Material Science, University of Swat, Khyber Pakhtunkhwa, Pakistan
Tabassam Razaq: Institute of Microbiology and Molecular Genetics, University of the Punjab, Quaid-e-Azam Campus, Lahore, Punjab, Pakistan
Samar A. Aldossari, Mohammed Sheikh Saleh Mushab: Department of Chemistry, College of Science, King Saud University, P. O. Box 2455, Riyadh, 11451, Saudi Arabia

1 Introduction

The need for smarter, smaller, and multiphase nanoparticles in the field of nanochemistry has given birth to a newly emergent class of compounds called nanocomposite materials [1]. For the last few decades, considerable attention has been given to the formation and development of nanocomposite materials as exclusive, functional nanomaterials with enhanced properties [2,3]. Antibiotic resistance is becoming a major global public health problem as a result of human abuse and disrespect, numerous studies have investigated the use of magnetic nanoparticles (MNPs) in bacterial infection control [4,5]. The study of magnetic ceramic composite and its use in the biomedical area has been one of the most fascinating issues for academics over the past 10 years [6]. Nanomaterials have been the subject of several studies utilizing magnetic hyperthermia up to this point, but for practical medical use, they present a number of inescapable difficulties, the most prevalent of which is early toxicity [7–9].

A wide range of illnesses affecting the human body with genetic abnormalities in cells which lead to uncontrolled cell division, which spreads to other body areas is referred to as cancer [10,11]. It is one of the most devastating and terrifying diseases that, regardless of prosperous or poor countries, results in significant fatalities globally [12,13]. The existing therapies for cancer treatments are mainly based on surgical operations, radiotherapy, chemotherapy, genetherapy, hormonotherapy, and immunotherapy, which badly affect the patient's life due to side effects associated with these therapies [14–16]. In conjunction with radiation or chemotherapy, magnetic hyperthermia is currently a popular cancer treatment option [17]. Hyperthermia is a type of non-invasive anticancer treatment in which a body part or tissue is subjected to an elevated temperature between 43 and 48°C to preferentially destroy or make the cancerous cells more susceptible to some other follow-up therapy [18–20]. The serious disadvantage associated with other therapies (IR radiation therapy, hot water, supersonic therapy, *etc.*) is that normal cells are also affected besides the cancerous cells. So therapies involving the heating of carcinomatous areas selectively and locally are strongly needed [21–23].

Many different materials have been created and tested to see how well they work in the treatment of cancer using hyperthermia. Bioactive ceramics have emerged as particularly beneficial among these materials [24,25]. As a typical bioactive substance, hydroxyapatite [$Ca_{10}(Po_4)_6(OH)_2$ or HA] is employed as bone cement, dental implants, drug delivery, and toothpaste ingredient due to its remarkable biocompatibility, osteoconductivity, bioactivity, chemical, and biological similarities with the mineral components of human bones and teeth [26–28]. The biocompatibility of magnetite (Fe_3O_4) nanoparticles with the human body is well recognized. Though, there is concern over the nanoparticle's potential for long-term toxicity, the most efficient way to solve this issue is to utilize magnetic Fe-doped HA; however, incorporating Fe_3O_4 nanoparticles into HA matrices can also lessen the long-term harmful effects [8,29,30].

Because of their ability to produce heat under a hyperthermic high-frequency alternating magnetic field, superparamagnetic nanoparticles have attracted a lot of interest. There have been several published studies on the usage of these particles in hyperthermia [6,31,32]. Despite the fact that these magnetite nanocomposites are target-directed and biocompatible with the human body, it is preferable to mix them with a suitable bioactive substrate to avoid any potential long-term negative effects. The most efficient method for treating malignant bone tumors with heat is to use HA composite materials that include magnetite [29,33–35]. They have also been used as adsorbents [36–39] and catalysts [40,41] in recent investigations. Additionally, it has been observed that MNPs (Fe_3O_4) can induce bactericidal properties by inhibiting bacterial growth and viability [42]. In particular, magnetite-incorporated HA nanocomposites have huge potential to be used in biomedical applications, especially in bone cancer where destruction of cancerous cells as well as regeneration of bone tissue is desired [43,44].

The traditional methods for creating HA-Fe_3O_4 nanocomposites have limitations since more ageing processes lead to the creation of these nanoparticles, which requires a longer reaction time. Thus, a straightforward procedure must be created for the quick formation of these bioactive nanocomposites with improved properties [29].

In this research, a simple unique one-pot continuous microwave flow synthesis methodology was used to create a variety of HA-Fe_3O_4 nanoparticles. Utilizing a variety of optical and analytical techniques, the structural characterization, and magnetic and antimicrobial properties of these newly created nanocomposites were assessed.

2 Materials and methods

For the synthesis of HA-Fe_3O_4 nanocomposite, iron source used was iron citrate ($C_6H_5O_7Fe{\cdot}3H_2O$, 98%), while diammonium hydrogen phosphate [$(NH_4)_2HPO_4$, 98%], calcium nitrate tetrahydrate [$Ca(NO_3)_2{\cdot}4H_2O$, 99%], and ammonium hydroxide solution (NH_4OH, 28 vol%) were used in the synthesis process. During all experimentation, deionized water was consumed.

2.1 Experimental method

2.1.1 Synthesis of hydroxyapatite

By using a continuous microwave-assisted flow synthesis (CMFS) technique, the pure nano-hydroxyapatite was synthesized at pH 10. In the synthesis process, the solutions of calcium nitrate (59 g) and diammonium hydrogen phosphate (19.8 g), were mixed together by pumping them at a flow rate of 20 mL min^{-1} to a T-piece during the continuous microwave assisted flow synthesis procedure. This original combination was linked to Teflon tubing of 8 m length, which was twisted into a household microwave oven (800 W) at low temperature, where the reaction was completed in 5 min. The white powder with ~85 % yield was the resulting product.

The suspension that was collected in a beaker from the exit point was centrifuged at 4,500 rpm for 10 min. The supernatant was removed, a VWR vortex mixer was used

to redistribute the wet residue in 45 mL deionized (DI) water for 5 min, following three additional centrifugation and washing sequences. The final product was obtained by freeze-drying the moist solid at 0.3 Pa for 24 h.

2.1.2 Synthesis of superparamagnetic Fe_3O_4 nanoparticles

Using a continuous flow synthesis method, Fe_3O_4 nanoparticles were produced quickly in a shorter time period of just 5 min at pH 11. Citric acid (11.52 g) and iron nitrate (20.2 g), were injected from opposite directions to meet at a "T"-shaped mixer during this procedure. The reaction between citric acid and iron nitrate was completed in 8 m long Teflon tubing for a duration of 5 min. The dark brown Fe_3O_4 precipitates were collected in a beaker, washed, spun in a centrifuge, and then freeze-dried.

2.1.3 Synthesis of HA-Fe_3O_4 nanocomposite

Using the CMFS technique as previously described, a variety of HA-Fe_3O_4 nanocomposites were created. The HA and Fe_3O_4 samples were run through the CMFS system to produce the nanocomposite materials. An 8 m Teflon tube was twisted inside a standard microwave oven with the original mixture attached, and the reaction took 5 min to complete. The resultant light brown precipitates were centrifuged and freeze-dried according to the procedure discussed in Sections 2.1.1 and 2.1.2 and as shown in Figure 1.

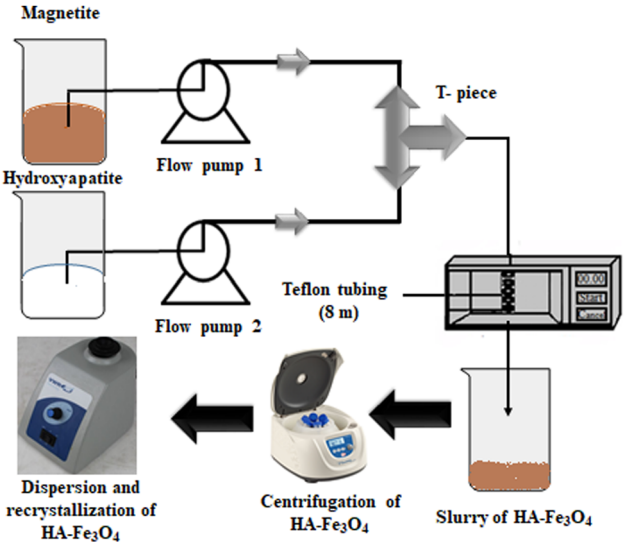

Figure 1: Schematic diagram for the preparation of HA-Fe_3O_4.

2.2 Characterization techniques

2.2.1 Powder X-ray diffraction (XRD)

All samples underwent XRD analysis using a Bruker-X-ray diffractometer. Cu-K radiations (λ = 1.5406 Å) were used to evaluate the data in the 2θ range from 10° to 70° with a scanning step of 0.05° and a count duration of 2 s. Phase analysis of the data was performed using DIFFRACplus Eva software by spectral matching with benchmark patterns. The Debye-Sherrer equation was used to compute the sizes of the crystallites.

2.2.2 Transmission electron microscopy (TEM)

An electron microscope made by JEOL, 100 CX was used for the TEM investigation. Dispersing a little quantity of material in methanol and ultrasonically processing it for 2 min produced a highly diluted suspension. The next step was to put a little amount of the suspension onto a carbon-coated copper grid (purchased from Agar Scientific), which served as the TEM specimen. Prior to using the grid in the TEM's double tilt holder, it was dried. Software for estimating particle size was installed, and it is version 5.0 of Image J.

2.2.3 Brunauer-Emmett-Teller (BET) surface area analysis

All samples' BET surface area (N_2 adsorption) measurements were made using a multipoint BET surface area analyzer. After being cleaned with methanol, the sample tubes were dried for a whole night at 100°C in the oven. Prior to BET analysis, the dried particles were precisely weighed and degassed at 180°C for 12 h. They were weighed again after degassing, followed by an analysis. Nitrogen physisorption at 196°C was used to estimate the BET surface area.

2.2.4 Zeta potential measurement

For the determination of the stability and surface charge of the fabricated magnetite nanocomposites, the Zeta potentials were calculated using the Anton Paar Particle Size Analyzer (Litesizer 500).

2.2.5 X-ray photoelectron spectroscopy (XPS) chemical composition

Thermo Scientific's XPS analyzer was used to conduct the chemical analysis. At the source, the X-rays were microfocused to produce spots on the sample that ranged in size from 30 to

400 microns. The vacuum chamber pressure was around 3×10^{-8} Torr, and the detector had 128 channel locations, making it a very sensitive device. For survey scans, the spectrum required 150 eV of energy, and for high-resolution regions, 50 eV. The CASA^{TM} program was used to process the XPS spectra.

2.2.6 Magnetic properties

The magnetization loops for magnetic nanocomposites were measured at 300 K using a vibrating sample VSM magnetometer. The powder samples above 10 mg were taken in sample holders for analysis. The heat changes in the HA-Fe_3O_4 nanocomposites were also measured using an alternating magnetic field of 600 kHz and 3.2 kA/m.

2.2.7 Antimicrobial assay

The antimicrobial potential of magnetite hydroxyapatite nanoparticles was examined using agar well diffusion technique [28,45]. *Escherichia coli* (ATCC 25922), a Gram-negative bacterium, was one of the four strains chosen for antibacterial screening, along with the Gram-positive bacteria *Staphylococcus aureus* (ATCC 25923), *Micrococcus luteus* (ATCC 49732), and *Bacillus subtilis* subsp. *spizizenii* (ATCC 6633). Reference antibiotic standards were used as a positive control [Ciprofloxacin (10 µg/mL) and Vancomycin (10 µg/mL)], while the negative control was HA. In 1 L of DI water, 28 g nutrient agar was suspended, mixed thoroughly by heating, followed by intermittent stirring, and then completely dissolved by boiling for 1 min. In an autoclave, sterilization was conducted for 15 min at 121°C and 15 psi. Sabouraud dextrose agar plates were used for screening of antifungal properties against *S. cerevisiae* (ATCC 9763). All samples were having a concentration of 150 µg/mL, the samples were weighed using a microanalytical balance. The sterilized agar suspension was poured into Petri plates, settled, and then incubated for 24 h. Each test bacteria's freshly prepared inoculum suspension was evenly distributed over the surface of the petri plates containing agar suspension. 50 µL of HA, 10HA-Fe_3O_4, 20HA-Fe_3O_4, and 30HA-Fe_3O_4 was placed into the each labelled well. The zones of inhibition were measured using a calibrated Vernier caliper after the samples and reference antibiotic standards were incubated at 37°C for 24 h (n = 3).

3 Results and discussion

In order to investigate the phase purity of pure HA sample, Powder XRD analysis was carried out. There were no extra

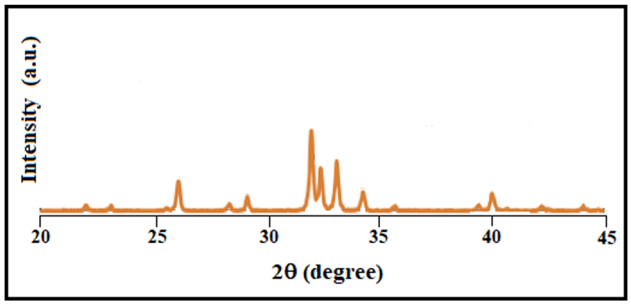

Figure 2: XRD analysis of pure HA synthesized using CMFS.

beta TCP peaks seen in the HA XRD patterns represented in Figure 2, which have an excellent match to JCPDS pattern 09-432 [46–48].

The phase purity and crystallinity of magnetite samples were also assessed from XRD measurements and were confirmed to be crystalline in nature. The XRD patterns of phase pure magnetite NPs are exhibited in Figure 2. No further diffraction peaks for other forms of iron oxide, such as α-Fe_2O_3 and Y-Fe_2O_3, were seen. Thus, the results revealed that the obtained nanoparticles are pure Fe_3O_4.

The HA-Fe_3O_4 nanopowder's XRD pattern exhibited strong agreement with stoichiometric hydroxyapatite (JCPDS 09-0432 card), with a little displacement of the angles that were presumably caused by an increase in magnetite concentration. As illustrated in Figure 3, the peaks at 35.43° and 43.05° correspond to magnetite in 10, 20, and 30 wt% HA-Fe_3O_4 confirmed by previous literature [29,40]. The crystallite sizes calculated using the Debye-Sherrer formula were found to be 58, 47, and 42 nm for 10HA-Fe_3O_4, 20HA-Fe_3O_4, and 10HA-Fe_3O_4, respectively.

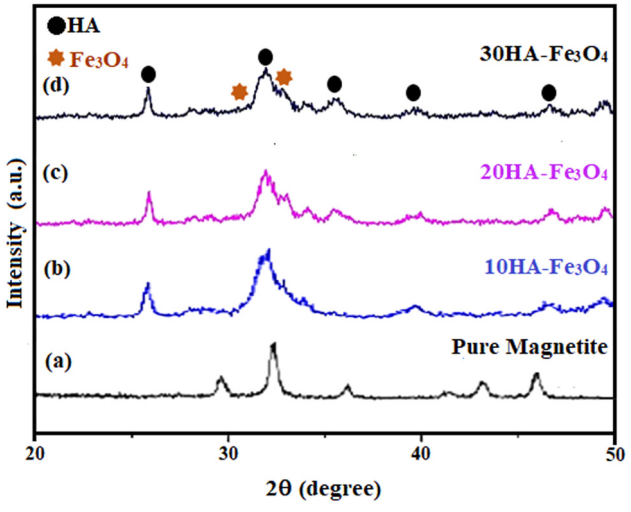

Figure 3: XRD pattern of HA-Fe_3O_4 nanocomposites: (a) Pure magnetite, (b) 10HA-Fe_3O_4, (c) 20HA-Fe_3O_4, and (d) 30HA-Fe_3O_4, prepared at pH 11 in 5 min in CMFS.

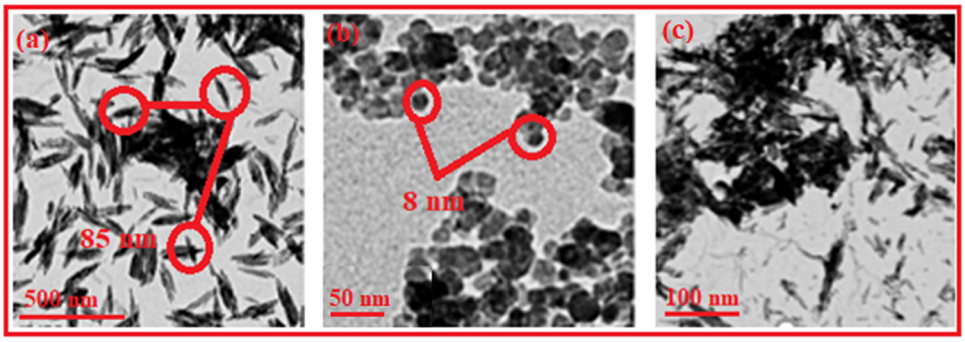

Figure 4: TEM images of (a) pure HA, (b) pure magnetite, and (c) HA-Fe_3O_4 nanocomposites.

The properties of nanocomposites exhibit a correlation with XRD-analyzed characteristics such as crystallinity, phase identification, magnetite content, and crystallite size [49]. When the crystallite size is small as in case of 30HA-Fe_3O_4, an enhanced antimicrobial activity and heat generation are measured.

The images of the samples taken under a transmission electron microscope, as seen in Figure 4, provided proof that tiny crystallites had been produced. Pure HA sample generated in 5 minutes of residence time by CMFS showed a mean particle size of 85 ± 15 nm (Figure 4a). The magnetite nanoparticles as prepared in pure phase had a spherical morphology with a mean particle size of 8 ± 1.8 nm observed by these nanoparticles. The total particle count was found to be 250 with a moderate agglomeration as depicted in Figure 4b. In nanocomposites of Fe_3O_4-HA, spherical magnetite structures had been observed on the surface of HA rods as shown in Figure 4c with a size of 41 ± 2 nm. The crystallite sizes calculated from XRD data using the Debye-Sherrer formula and from TEM images were almost in accordance with each other. The previously reported size of spherical magnetite nanoparticles and magnetite hydroxyapatite is 75.34 ± 5.56 nm, and 95.16 ± 14.92 nm, respectively [8]. TEM analysis offers insights into particle size distribution, impacting properties such as drug release rates or magnetic responsiveness [50]. TEM analysis of nanocomposites indicates a direct link between their characteristics and hyperthermia as well as antimicrobial efficacy. The size and shape of these nanocomposites significantly impact their heating efficiency when subjected to magnetic fields [51]. Typically, smaller and uniformly shaped particles exhibit a higher capacity to generate heat, 30HA-Fe_3O_4 are in complete agreement to this statement. Conversely, the structural features of these nanocomposites enhance the bacterial adhesion which leads to membrane disruption [52].

The BET surface area analysis was also performed for "as precipitated" amorphous HA-Fe_3O_4 samples prepared in 5 min of residence time. It was observed that the HA-Fe_3O_4 nanocomposite had a surface area of 122.4, 139.5, and 156.3 $m^2 g^{-1}$ for the samples 10, 20, and 30 wt% respectively as represented in Table 1. It could be concluded that with the increase in the concentration of magnetite, the surface area of HA-Fe_3O_4 increases [53]. The BET surface area analysis comprehends the interaction of nanocomposites with the surrounding molecules or cells. In biomedical applications, a larger surface area typically denotes enhanced cell adhesion or better drug loading capability [54].

Zeta potential, which reveals the electrostatic potential of the particles and is directly correlated with the stability of their dispersion through electrostatic repulsion, is a parameter to measure colloidal stability.

Higher zeta potential levels correspond to higher colloidal stability of the suspension resulting from increased electrostatic repulsion. Zeta potential measurements for HA-Fe_3O_4 nanocomposite at 10, 20, and 30 wt% revealed strong negative surface charges with values of −18.9, −21.9, and −24.6 mV, respectively, confirmed by previous literature [55]. A more stable dispersion has resulted from the higher value of zeta potential indicating a higher surface charge,

Table 1: BET, TEM, zeta potential, and magnetization values of HA-Fe_3O_4

Sample ID	XRD crystallite (nm)	BET ($m^2 g^{-1}$)	TEM (nm)	Zeta potential (mV)	Magnetization (emu/g)
10HA-Fe_3O_4	58	122.4	56	−18.9	—
20HA-Fe_3O_4	47	139.5	49	−21.9	–
30HA-Fe_3O_4	42	156.3	41	−24.6	59

which inhibits the aggregation of the particles. When evaluating the biological interactions and therapeutic efficacy of nanocomposites, surface charge plays a pivotal role. Positively charged nanocomposites are drawn towards the negatively charged cell membrane *via* electrostatic forces, facilitating rapid cellular uptake. Conversely, negatively charged nanocomposites might have an easier time targeting specific organs or receptors [56]. The accumulation of nanocomposites in particular tissues or organs can be influenced by their surface charge. For instance, negatively charged particles tend to target tumors more effectively, while positively charged ones often accumulate in the liver and spleen [57]. Surface charge also governs drug release from nanocomposites; pH-sensitive charges, for instance, enable controlled medication release, especially in environments like tumors [58].

The investigation of the concentration of the magnetite, its oxidation state, and its impact on the architecture of the lattice was achieved by XPS experiments. Figure 5 displays a typical survey spectrum for pure HA and 10HA-Fe_3O_4 nanocomposites. The P 2p peak of phosphate groups in HA were identified at 134 eV. O 1s, Ca 2p, and C 2s′ binding energies were calculated to be 533, 347, and 285 eV, individually. A smaller intensity at 710 eV corresponding to Fe 2p, which is missing in pure HA, was also reported previously [40,59]. As XPS provides important insights into the syrface chemistry and interfacial interactions of a nanocomposite by determining its elemental composition and chemical state, these findings profoundly influence interactions between biological fluids or other materials [60]. XPS does not directly correlate with hyperthermia or antimicrobial activity. However, the oxidation states of iron in magnetite can significantly impact its magnetic properties, which are essential for hyperthermia applications. Moreover, XPS has confirmed the presence of both HA and Fe_3O_4, and it is established that both components contribute to antimicrobial activity [52].

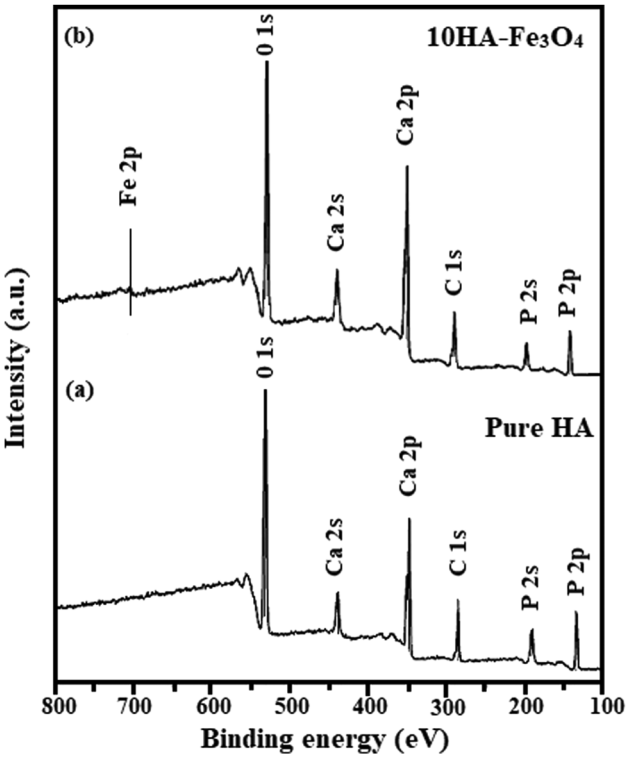

Figure 5: The XPS survey spectrum of (a) Pure HA and (b) 10HA-Fe_3O_4 nanocomposite.

Figure 6a shows the hysteresis loops of the Fe_3O_4 nanoparticles observed at 300 K. Fe_3O_4 nanoparticle saturation magnetization values Ms at 300 K were found to be 70 emu/g, respectively. According to the findings, as shown in Figure 6b, the saturation magnetization value in 30HA-Fe_3O_4 nanocomposites reduced to 59 emu/g from pure magnetite. HA-Fe_3O_4 is widely dispersed in the composite structure across the single pure phase and shows superparamagnetism, as is displayed from VSM measurements [61]. The reduction in Ms value has resulted from the diamagnetic behavior of HA while the superparamagnetic behavior of HA-Fe_3O_4 is due to the lack of a hysteresis loop [62–64].

Superparamagnetic magnetite nanoparticles have the ability to produce magnetism once placed in a magnetic field. This ability of heat generation at a specific temperature of about 43°C can be used to destroy cancer cells [65,66]. It was observed that the 10 and 20HA-Fe_3O_4 nanocomposites were unable to produce enough heat for anticancer therapy. However, the magnetic apatite composites with 30 wt% magnetite concentrations exhibited a temperature of 51°C in 10 min, which is sufficient enough to destroy cancer cells during hyperthermia therapy for bone cancer. It can be inferred that increasing the concentration of magnetite in HA-Fe_3O_4, a significant increase in temperature can be achieved. Therefore, a synergistic behavior significantly dependent on concentration and particle size can be observed between HA and magnetite. Thus, the newly developed, highly magnetic magnetite incorporated HA nanocomposites can be used as an efficient tool for various cancer therapies and in addition for bone regeneration applications due to the strong bone-bonding ability of HA. High magnetization is a significant factor for the effective operation of MNPs across various applications, including magnetic hyperthermia. Enhanced magnetization heightens MNPs' susceptibility to magnetic forces, enabling precise manipulation in both technical and biological contexts. This attribute empowers MNPs to respond markedly to external magnetic fields, a pivotal aspect in their functionality. This elevated magnetization ensures

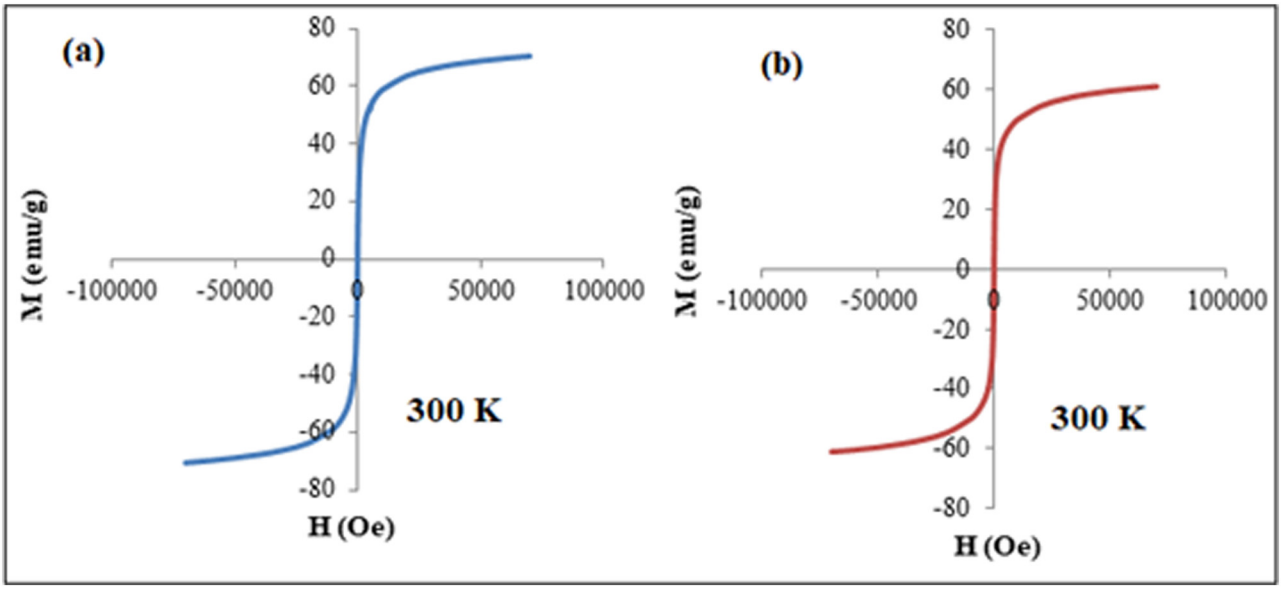

Figure 6: The saturation magnetization values Ms of (a) pure Fe_3O_4 nanoparticles and (b) 30HA-Fe_3O_4 nanocomposites, respectively, at 300 K.

that MNPs efficiently convert applied magnetic field energy into heat during hyperthermia therapy. As a result, targeted tissues experience a rise in temperature, enabling therapeutic effects [67,68].

Four bacterial and one fungal strain were used in the evaluation of the antimicrobial characteristics of the pure HA, Fe_3O_4, 10HA-Fe_3O_4, 20HA-Fe_3O_4, and 30HA-Fe_3O_4. The results were highly encouraging. These are the typical prokaryotic microorganisms that have been linked to a variety of illnesses in both humans and animals. The results in Table 2 suggest that the synthesized nanocomposites were more effective against gram-negative bacteria than gram-positive bacteria. 30HA-Fe_3O_4 demonstrated the highest efficacy against *E. coli* (20.000 ± 0.25 mm) and *S. cerevisiae* exceeding the bacterial inhibition capacity of the widely used antibiotics ciprofloxacin and vancomycin.

From the data in Table 2 it could be assumed that as the concentration of Fe_3O_4-HA nanocomposite increases, *E. coli* and *S. aureus* cells gradually lose their integrity [55]. A comparative antimicrobial assay of HA-Fe_3O_4 nanocomposites is illustrated in Figure 7, the calculated values are considerably closer to the real values ($p < 0.05$) after applying a hypothetical t-test using OriginPro software. According to the literature, the release of OH^- ions in an aqueous environment is linked to HA's antimicrobial action. Due to their high oxidizing ability, they react with a wide range of biomolecules. These free radicals hardly diffuse away from the sites of generation due to their strong and indiscriminate reactivity [5]. In the presence of Fe_3O_4-HA, the cell structure of bacteria is affected, the increase in the concentration of HA-Fe_3O_4 increases the rate of cell membrane damage as more nanocomposites come in contact with the bacterial cell [69]. Some proposed mechanisms suggest that due to the generation of reactive oxidative species (ROS), the nanoparticles diffuse into bacterial cells and obstruct their metabolic processes. They can also interact directly with bacterial DNA or thiol groups in proteins to halt all functions and cause cell death, or they can react with

Table 2: Antibacterial assay of pure HA and varied concentrations of Fe_3O_4-HA

Bactria/Fungi	Zone of inhibition (mm)					
	Ciprofloxacin	Vancomycin	Fe_3O_4	10HA-Fe_3O_4	20HA-Fe_3O_4	30HA-Fe_3O_4
E. coli	17.417 ± 0.04	17.817 ± 0.21	11.613 ± 0.21	14.613 ± 0.29	16.630 ± 0.32	20.000 ± 0.25
S. aureus	15.623 ± 0.06	17.130 ± 0.08	7.537 ± 0.25	11.537 ± 0.24	13.303 ± 0.77	15.410 ± 0.76
B. spizizenii	15.637 ± 0.10	16.430 ± 0.52	8.763 ± 0.33	9.763 ± 0.39	10.990 ± 0.69	11.453 ± 0.95
M. luteus	18.423 ± 0.37	19.427 ± 0.06	8.833 ± 0.26	9.833 ± 0.33	9.730 ± 0.32	9.887 ± 0.39
S. cerevisiae	11.380 ± 0.06	10.083 ± 0.24	10.050 ± 0.56	14.050 ± 0.66	14.667 ± 1.04	15.913 ± 0.40

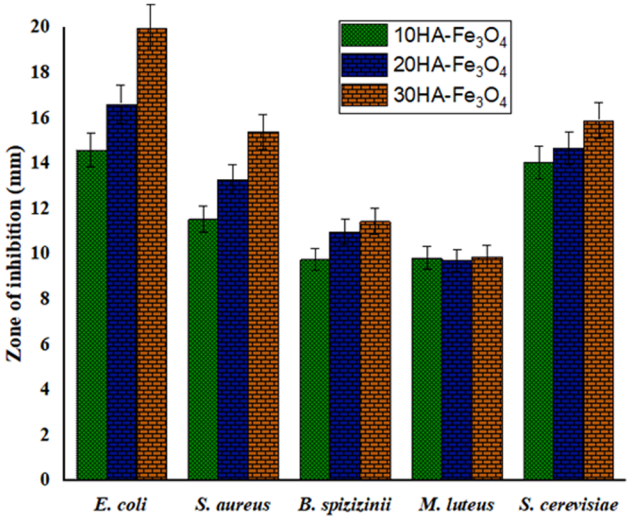

Figure 7: Antimicrobial activity of various concentrations of HA-Fe_3O_4.

the cell wall and membrane of the bacterial cell to create holes through which the cellular contents leak out [45,53,70,71]. All concentrations of Fe_3O_4-HA have depicted strong activity against *S. cerevisiae*. As the saturation of the solution rises, the fungus becomes dormant and loses its ability to cling to fungal hyphae owing to high density. By rupturing cell walls and membranes, impeding mycelial development and conidial germination, and producing ROS, the nanoparticles prevent the growth of fungus [72].

Precise optimization of synthesis parameters (flow rate, microwave power, temperature) was achieved after a series of reactions with careful observations. The optimization was significant in acquiring desired nanocomposite properties within a short residence time [73,74]. Microwaves penetrate the reaction mixture, leading to volumetric heating and accelerating reaction kinetics. This enables faster synthesis compared to conventional methods. Continuous flow ensures efficient mixing and transport of reactants, promoting rapid nucleation and growth of nanoparticles. Short residence time allows for fine-tuning of particle size, shape, and composition by adjusting flow rate and microwave power [75]. Shorter synthesis time reduces energy consumption. Shorter residence time results in smaller, more uniform nanoparticles beneficial for certain applications, such as drug delivery, where smaller particles can enhance bioavailability. It also ensures the preservation of magnetite's magnetic properties, essential for applications such as magnetic separation or hyperthermia. Extremely good results were obtained using the unique CMFS method, this work provided the fastest method for producing extremely thin nanorods of pure and Fe_3O_4 substituted bioactive nanobioceramics with a large surface area in a relatively short period of time. The synthesis method and increasing concentration of Fe_3O_4 has greatly improved the hyperthermal properties of the magnetic HA-Fe_3O_4.

4 Conclusion

Magnetic HA-Fe_3O_4 nanocomposites were successfully fabricated with varied percentage compositions in only 5 min of residence time without any stirring and aging using continuous microwave flow synthesis. 30HA-Fe_3O_4 nanocomposites have shown very promising results with high surface area 156.3 $m^2 g^{-1}$, small particle size (41 nm), and negative surface charge (−24.6 mV). The superparamagnetic MNPs have a heat generation of 51°C within 10 min after placing in magnetic field; therefore, they can be employed as an efficient tool for various cancer therapies. Remarkable antimicrobial properties have been revealed by HA-Fe_3O_4 nanocomposites. As a result of better magnetic properties and high magnetization values, they can improve the sintering kinetics. Hence, HA-Fe_3O_4 composites produced through our synthesis approach can effectively treat malignant bone tumors with heat. Ample effort would be put into creating HA-Fe_3O_4 nanocomposites having large surface area with tunable mechanical and magnetic properties for bone tissue regeneration, fabrication of highly sensitive and specific biosensors for early disease diagnosis and *in vivo* studies for utilization in the future.

Funding information: This work was supported by the National Research Foundation of Korea (NRF) grant funded by the Korea government (MSIT) (No. 2022R1C1C1008831). This study has been conducted with the support of the Korea Institute of Industrial Technology as "Development of intelligent root technology with add-on modules (KITECH EO-23-0005)." This research was supported by the Ministry of Trade, Industry, and Energy (MOTIE) of Korea through the "Innovative Digital Manufacturing Platform" (project no. P0022331) supervised by the Korea Institute for Advancement of Technology (KIAT). The work was supported by Researchers Supporting Project number (RSPD2024R663), King Saud University, Riyadh, Saudi Arabia.

Author contributions: All authors have accepted responsibility for the entire content of this manuscript and approved its submission.

Conflict of interest: The authors state no conflict of interest.

References

[1] Al-Mutairi NH, Mehdi AH, Kadhim BJ. Nanocomposites materials definitions, types and some of their applications: A review. Eur J Res Dev Sustain. 2022;3(2):102–8.

[2] Okpala CC. The benefits and applications of nanocomposites. Int J Adv Eng Tech. 2014;12:18.

[3] AbuShanab WS, Moustafa EB, Taha MA, Youness RA. Synthesis and structural properties characterization of titania/zirconia/calcium silicate nanocomposites for biomedical applications. Appl Phys A. 2020;126:1–12.

[4] Mosaiab T, Jeong CJ, Shin GJ, Choi KH, Lee SK, Lee I, et al. Recyclable and stable silver deposited magnetic nanoparticles with poly (vinyl pyrrolidone)-catechol coated iron oxide for antimicrobial activity. Mater Sci Eng C. 2013;33(7):3786–94.

[5] Rad Goudarzi M, Bagherzadeh M, Fazilati M, Riahi F, Salavati H, Shahrokh Esfahani S. Evaluation of antibacterial property of hydroxyapatite and zirconium oxide-modificated magnetic nanoparticles against Staphylococcus aureus and Escherichia coli. IET Nanobiotechnolog. 2019;13(4):449–55.

[6] Bretcanu O, Miola M, Bianchi CL, Marangi I, Carbone R, Corazzari I, et al. In vitro biocompatibility of a ferrimagnetic glass-ceramic for hyperthermia application. Mater Sci Eng C. 2017;73:778–87.

[7] Miola M, Pakzad Y, Banijamali S, Kargozar S, Vitale-Brovarone C, Yazdanpanah A, et al. Glass-ceramics for cancer treatment: so close, or yet so far? Acta Biomater. 2019;83:55–70.

[8] Mondal S, Manivasagan P, Bharathiraja S, Santha Moorthy M, Kim HH, Seo H, et al. Magnetic hydroxyapatite: A promising multifunctional platform for nanomedicine application. Int J Nanomed. 2017;8389–410.

[9] Mushtaq A, Zhao R, Luo D, Dempsey E, Wang X, Iqbal MZ, et al. Magnetic hydroxyapatite nanocomposites: The advances from synthesis to biomedical applications. Mater Des. 2021;197:109269.

[10] Kumar A, Vashist H, Sharma R, Garg D. An anthology of cancer. IIJMPS. 2018;3(4):7–14.

[11] Baskar R, Lee KA, Yeo R, Yeoh K-W. Cancer and radiation therapy: Current advances and future directions. Int J Med Sci. 2012;9(3):193.

[12] Mahmoodzadeh F, Hosseinzadeh M, Jannat B, Ghorbani M. Fabrication and characterization of gold nanospheres-cored pH-sensitive thiol-ended triblock copolymer: A smart drug delivery system for cancer therapy. Polym Adv Technol. 2019;30(6):1344–55.

[13] Danewalia S, Singh K. Bioactive glasses and glass–ceramics for hyperthermia treatment of cancer: State-of-art, challenges, and future perspectives. Mater Today Bio. 2021;10:100100.

[14] Sneha M, Sundaram NM, Kandaswamy A. Synthesis and characterization of magnetite/hydroxyapatite tubes using natural template for biomedical applications. Bull Mater Sci. 2016;39:509–17.

[15] Baronzio G, Parmar G, Ballerini M, Szasz A, Baronzio M, Cassutti V. A brief overview of hyperthermia in cancer treatment. J Integr Oncol. 2014;3(115):2.

[16] Yu S, He C, Chen X. Injectable hydrogels as unique platforms for local chemotherapeutics-based combination antitumor therapy. Macromol Biosci. 2018;18(12):1800240.

[17] Mondal S, Manivasagan P, Bharathiraja S, Santha Moorthy M, Nguyen VT, Kim HH, et al. Hydroxyapatite coated iron oxide nanoparticles: A promising nanomaterial for magnetic hyperthermia cancer treatment. Nanomaterials. 2017;7(12):426.

[18] Seynhaeve A, Amin M, Haemmerich D, Van Rhoon G, Ten Hagen T. Hyperthermia and smart drug delivery systems for solid tumor therapy. Adv Drug Deliv Rev. 2020;163:125–44.

[19] Aslibeiki B, Eskandarzadeh N, Jalili H, Varzaneh AG, Kameli P, Orue I, et al. Magnetic hyperthermia properties of $CoFe_2O_4$ nanoparticles: Effect of polymer coating and interparticle interactions. Ceram Int. 2022;48(19):27995–8005.

[20] Wust P, Hildebrandt B, Sreenivasa G, Rau B, Gellermann J, Riess H, et al. Hyperthermia in combined treatment of cancer. Lancet Oncol. 2002;3(8):487–97.

[21] Di Corato R, Espinosa A, Lartigue L, Tharaud M, Chat S, Pellegrino T, et al. Magnetic hyperthermia efficiency in the cellular environment for different nanoparticle designs. Biomaterials. 2014;35(24):6400–11.

[22] Cho M, Cervadoro A, Ramirez MR, Stigliano C, Brazdeikis A, Colvin VL, et al. Assembly of iron oxide nanocubes for enhanced cancer hyperthermia and magnetic resonance imaging. Nanomaterials. 2017;7(4):72.

[23] Dahaghin A, Emadiyanrazavi S, Haghpanahi M, Salimibani M, Bahreinizad H, Eivazzadeh-Keihan R, et al. A comparative study on the effects of increase in injection sites on the magnetic nanoparticles hyperthermia. Int J Drug Deliv Technol. 2021;63:102542.

[24] Miola M, Gerbaldo R, Laviano F, Bruno M, Vernè E. Multifunctional ferrimagnetic glass–ceramic for the treatment of bone tumor and associated complications. J Mater Sci. 2017;52:9192–201.

[25] Baino F, Fiume E, Miola M, Leone F, Onida B, Laviano F, et al. Fe-doped sol-gel glasses and glass-ceramics for magnetic hyperthermia. Materials. 2018;11(1):173.

[26] Wang M-C, Chen H-T, Shih W-J, Chang H-F, Hon M-H, Hung I-M. Crystalline size, microstructure and biocompatibility of hydroxyapatite nanopowders by hydrolysis of calcium hydrogen phosphate dehydrate (DCPD). Ceram Int. 2015;41(2):2999–3008.

[27] Kamonwannasit S, Futalan C, Khemthong P, Butburee T, Karaphun A, Phatai P. Synthesis of copper-silver doped hydroxyapatite via ultrasonic coupled sol-gel techniques: structural and antibacterial studies. JSST. 2020;96:452–63.

[28] Anwar A, Akbar S, Sadiqa A, Kazmi M. Novel continuous flow synthesis, characterization and antibacterial studies of nanoscale zinc substituted hydroxyapatite bioceramics. Inorg Chim Acta. 2016;453:16–22.

[29] Iwasaki T, Nakatsuka R, Murase K, Takata H, Nakamura H, Watano S. Simple and rapid synthesis of magnetite/hydroxyapatite composites for hyperthermia treatments via a mechanochemical route. Int J Mol Sci. 2013;14(5):9365–78.

[30] Ebadi M, Rifqi Md Zain A, Tengku Abdul Aziz TH, Mohammadi H, Tee CAT, Rahimi Yusop M. Formulation and characterization of Fe_3O_4@ PEG nanoparticles loaded sorafenib; molecular studies and evaluation of cytotoxicity in liver cancer cell lines. Polymers. 2023;15(4):971.

[31] Ereath Beeran A, Fernandez FB, Varma PH. Self-controlled hyperthermia & MRI contrast enhancement via iron oxide embedded hydroxyapatite superparamagnetic particles for theranostic application. ACS Biomater Sci Eng. 2018;5(1):106–13.

[32] Palzer J, Eckstein L, Slabu I, Reisen O, Neumann UP, Roeth AA. Iron oxide nanoparticle-based hyperthermia as a treatment option in various gastrointestinal malignancies. Nanomaterials. 2021;11(11):3013.

[33] Bañobre-López M, Piñeiro-Redondo Y, De Santis R, Gloria A, Ambrosio L, Tampieri A, et al. Poly (caprolactone) based magnetic scaffolds for bone tissue engineering. J Appl Phys. 2011;109(7):07B313.

[34] Tampieri A, D'Alessandro T, Sandri M, Sprio S, Landi E, Bertinetti L, et al. Intrinsic magnetism and hyperthermia in bioactive Fe-doped hydroxyapatite. Acta Biomater. 2012;8(2):843–51.

[35] Gloria A, Russo T, d'Amora U, Zeppetelli S, d'Alessandro T, Sandri M, et al. Magnetic poly (ε-caprolactone)/iron-doped hydroxyapatite nanocomposite substrates for advanced bone tissue engineering. J R Soc Interface. 2013;10(80):20120833.
[36] Choi J-W, Lee H-K, Choi S-J. Magnetite double-network composite using hydroxyapatite-manganese dioxide for Sr2+ removal from aqueous solutions. J Env Chem Eng. 2021;9(4):105360.
[37] Li R, Liu Y, Lan G, Qiu H, Xu B, Xu Q, et al. Pb (II) adsorption characteristics of magnetic GO-hydroxyapatite and the contribution of GO to enhance its acid resistance. J Env Chem Eng. 2021;9(4):105310.
[38] Hui KC, Kamal NA, Sambudi NS, Bilad MR, editors. Magnetic hydroxyapatite for batch adsorption of heavy metals. E3S Web of Conferences. EDP Sciences; 2021.
[39] Elkady M, Shokry H, Hamad H. Microwave-assisted synthesis of magnetic hydroxyapatite for removal of heavy metals from groundwater. Chem Eng Technol. 2018;41(3):553–62.
[40] Biedrzycka A, Skwarek E, Hanna UM. Hydroxyapatite with magnetic core: Synthesis methods, properties, adsorption and medical applications. Adv Colloid Interface Sci. 2021;291:102401.
[41] Nabizad M, Dadvand Koohi A, Erfanipour Z. Removal of cefixime using heterogeneous fenton catalysts: Alginate/magnetite hydroxyapatite nanocomposite. JWENT. 2022;7(1):14–30.
[42] Tran N, Mir A, Mallik D, Sinha A, Nayar S, Webster T. Bactericidal effect of iron oxide nanoparticles on Staphylococcus aureus. Int J Nanomed. 2010;5:277–83.
[43] MehakThummer RP, Pandey LM. Surface modified iron-oxide based engineered nanomaterials for hyperthermia therapy of cancer cells. BGER. 2023;1–47.
[44] Leonel AG, Mansur HS, Mansur AA, Caires A, Carvalho SM, Krambrock K, et al. Synthesis and characterization of iron oxide nanoparticles/carboxymethyl cellulose core-shell nanohybrids for killing cancer cells in vitro. Int J Biol Macromol. 2019;132:677–91.
[45] Sadiqa A, Gilani SR, Anwar A, Mehboob A, Saleem A, Rubab S. Biogenic fabrication, characterization and drug loaded antimicrobial assay of silver nanoparticles using Centratherum anthalminticum (L.) Kuntze. J Pharm Sci. 2021;110(5):1969–78.
[46] Kusuma H, Sifah L, Anggita S, editors. The characterization of hydroxyapatite from blood clam shells and eggs shells: Synthesis by hydrothermal method. J Phys: Conf Ser. 2021. IOP Publishing.
[47] El Boujaady H, Mourabet M, El Rhilassi A, Bennani-Ziatni M, El Hamri R, Taitai A. Adsorption of a textile dye on synthesized calcium deficient hydroxyapatite (CDHAp): Kinetic and thermodynamic studies. J Mater Environ Sci. 2016;7(11):4049–63.
[48] Anwar A, Kanwal Q, Akbar S, Munawar A, Durrani A, Hassan Farooq M. Synthesis and characterization of pure and nanosized hydroxyapatite bioceramics. Nanotechnol Rev. 2017;6(2):149–57.
[49] de Jesús Ruíz-Baltazar Á, Reyes-López SY, Silva-Holguin PN, Larrañaga D, Estévez M, Pérez R. Novel biosynthesis of Ag-hydroxyapatite: Structural and spectroscopic characterization. Results Phys. 2018;9:593–7.
[50] Mathaes R, Winter G, Siahaan TJ, Besheer A, Engert J. Influence of particle size, an elongated particle geometry, and adjuvants on dendritic cell activation. Eur J Pharm Biopharm. 2015;94:542–9.
[51] Ali I, Jamil Y, Khan SA, Pan Y, Shah AA, Chandio AD, et al. Magnetic hyperthermia and antibacterial response of $CuCo_2O_4$ nanoparticles synthesized through laser ablation of bulk alloy. Magnetochemistry. 2023;9(3):68.
[52] Rad Goudarzi M, Bagherzadeh M, Fazilati M, Riahi F, Salavati H, Shahrokh Esfahani S. Evaluation of antibacterial property of hydroxyapatite and zirconium oxide-modificated magnetic nanoparticles against Staphylococcus aureus and Escherichia coli. IET Nanobiotechnol. 2019;13(4):449–55.
[53] Bajpai I, Balani K, Basu B. Synergistic effect of static magnetic field and HA-Fe_3O_4 magnetic composites on viability of S. aureus and E. coli bacteria. J Biomed Mater Res - B Appl Biomater. 2014;102(3):524–32.
[54] Bhatt A, Sakai K, Madhyastha R, Murayama M, Madhyastha H, Rath SN. Biosynthesis and characterization of nano magnetic hydroxyapatite (nMHAp): An accelerated approach using simulated body fluid for biomedical applications. Ceram Int. 2020;46(17):27866–76.
[55] Sahoo JK, Konar M, Rath J, Kumar D, Sahoo H. Magnetic hydroxyapatite nanocomposite: Impact on Eriochrome black-T removal and antibacterial activity. J Mol Liq. 2019;294:111596.
[56] Jo DH, Kim JH, Lee TG, Kim JH. Size, surface charge, and shape determine therapeutic effects of nanoparticles on brain and retinal diseases. Nanomedicine: NBM. 2015;11(7):1603–11.
[57] Chenthamara D, Subramaniam S, Ramakrishnan SG, Krishnaswamy S, Essa MM, Lin F-H, et al. Therapeutic efficacy of nanoparticles and routes of administration. Biomater Res. 2019;23(1):1–29.
[58] Bamburowicz-Klimkowska M, Poplawska M, Grudzinski IP. Nanocomposites as biomolecules delivery agents in nanomedicine. J Nanobiotechnology. 2019;17:1–32.
[59] Foroutan R, Peighambardoust SJ, Hemmati S, Ahmadi A, Falletta E, Ramavandi B, et al. Zn^{2+} removal from the aqueous environment using a polydopamine/hydroxyapatite/Fe_3O_4 magnetic composite under ultrasonic waves. RSC Adv. 2021;11(44):27309–21.
[60] Korin E, Froumin N, Cohen S. Surface analysis of nanocomplexes by X-ray photoelectron spectroscopy (XPS). ACS Biomater Sci Eng. 2017;3(6):882–9.
[61] Ebadi M, Bullo S, Buskara K, Hussein MZ, Fakurazi S, Pastorin G. Release of a liver anticancer drug, sorafenib from its PVA/LDH- and PEG/LDH-coated iron oxide nanoparticles for drug delivery applications. Sci Rep. 2020;10(1):1–19.
[62] Ali MAEAA, Hamad H. Synthesis and characterization of highly stable superparamagnetic $CoFe_2O_4$ nanoparticles as a catalyst for novel synthesis of thiazolo [4, 5-b] quinolin-9-one derivatives in aqueous medium. J Mol Catal A: Chem. 2015;404:148–55.
[63] Boda SK, Thrivikraman G, Basu B. Magnetic field assisted stem cell differentiation–role of substrate magnetization in osteogenesis. J Mater Chem B. 2015;3(16):3150–68.
[64] Ganapathe LS, Mohamed MA, Mohamad Yunus R, Berhanuddin DD. Magnetite (Fe_3O_4) nanoparticles in biomedical application: From synthesis to surface functionalisation. Magnetochemistry. 2020;6(4):68.
[65] Hilger I, Frühauf K, Andrä W, Hiergeist R, Hergt R, Kaiser WA. Heating potential of iron oxides for therapeutic purposes in interventional radiology. Acad Radiol. 2002;9(2):198–202.
[66] Jose J, Kumar R, Harilal S, Mathew GE, Parambi DGT, Prabhu A, et al. Magnetic nanoparticles for hyperthermia in cancer treatment: an emerging tool. Env Sci Pollut Res. 2020;27:19214–25.
[67] Vargas-Ortiz JR, Gonzalez C, Esquivel K. Magnetic iron nanoparticles: Synthesis, surface enhancements, and biological challenges. Processes. 2022;10(11):2282.
[68] Ali A, Shah T, Ullah R, Zhou P, Guo M, Ovais M, et al. Review on recent progress in magnetic nanoparticles: Synthesis, characterization, and diverse applications. Front Chem. 2021;9:629054.

[69] Mirzakhanlou H, Khoshnevis Zadeh R, Zare Karizi S. Prepration of pipractam liposomal formulations and evaluation of antimicrobial effect on Pseudomonas aeruginosa. Cell Mol Res (Iran J Biol). 2022;35(4):527–41.
[70] Tripathi D, Modi A, Narayan G, Rai SP. Green and cost effective synthesis of silver nanoparticles from endangered medicinal plant Withania coagulans and their potential biomedical properties. Mater Sci Eng C. 2019;100:152–64.
[71] Medina-Ramirez I, Luo Z, Bashir S, Mernaugh R, Liu JL. Facile design and nanostructural evaluation of silver-modified titania used as disinfectant. Dalton Trans. 2011;40(5):1047–54.
[72] Kim SW, Jung JH, Lamsal K, Kim YS, Min JS, Lee YS. Antifungal effects of silver nanoparticles (AgNPs) against various plant pathogenic fungi. Mycobiology. 2012;40(1):53–8.
[73] Anwar A, Akbar S. Novel continuous microwave assisted flow synthesis of nanosized manganese substituted hydroxyapatite. Ceram Int. 2018;44(9):10878–82.
[74] Anwar A, Akbar S, Kazmi M, Sadiqa A, Gilani SR. Novel synthesis and antimicrobial studies of nanoscale titania particles. Ceram Int. 2018;44(17):21170–5.
[75] Anwar A, Akbar S. Continuous microwave assisted flow synthesis and characterization of calcium deficient hydroxyapatite nanorods. Adv Powder Technol. 2018;29(6):1493–8.